A comparison of C^0 and G^1 continuous curved tetrahedral meshes for high-order finite element simulations

Daniel W. Zaide, Qiukai Lu, and Mark Shephard

Scientific Computation Research Center, Rensselaer Polytechnic Institute

October 12th, 2015

Introduction

Finite element methods are sensitive to the accuracy and smoothness of the mesh that approximates the curved domain boundaries.

Increasing interelement continuity has demonstrated increased accuracy on quadrilateral and hexahedral meshes.

We perform a preliminary study of the effects of surface triangle continuity, comparing a C^0 continuous surface with a G^1 continuous surface representation.
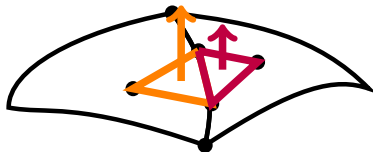
Surface Continuity

Consider two adjacent boundary triangles with tangent planes across their shared edge illustrated.
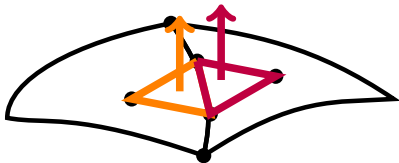
C^0 continuity
normals not in same
direction
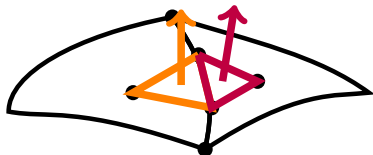
G^1 continuity
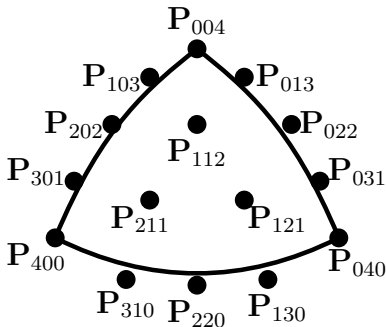normals in same direction,
different magnitude

C^1 continuity,
normals in same direction,
same magnitude

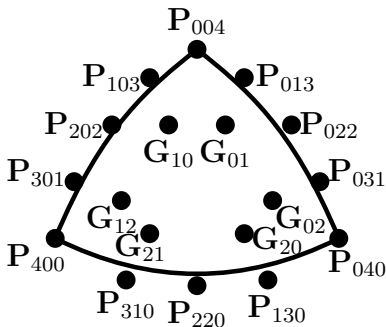# 4th Order Bézier Triangle

C^0 continuity obtained from the Bézier triangle,
4th order being the minimum needed for G^1 continuity.

$$\mathbf{B}(u, v, w) = \sum_{i+j+k=4} \frac{4!}{i!j!k!} u^i v^j w^k \mathbf{P}_{ijk}$$

G^1 Continuous Triangle

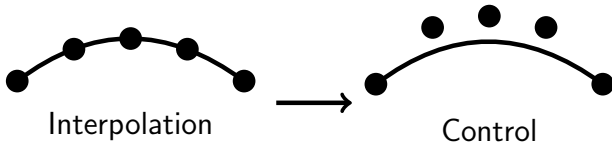G^1 continuity obtained from the 4th order triangle of Walton and Meek,

And can be computed using the 4th order Bézier equation, blending pairs of points to form the internal Bézier points, e.g.

$$\mathbf{P}_{112} = \frac{1}{v + w}(v\mathbf{G}_{12} + w\mathbf{G}_{21})$$

Mesh Curving

On CAD geometry, Bézier control points are calculated from interpolation points.

Interpolation points are from surface parametrization using the optimal locations of Chen and Babuška.

For G^1 control points, the algorithm of Walton and Meek is used except on CAD edges, where edge tangents are used instead of surface normals.

Blended Tetrahedron

The tetrahedral mapping we use the blending approach of Dey et al., to account for differences in exterior and interior shape functions, specifically from G^1 surface triangles.

$$
\begin{aligned}
x_i(\boldsymbol{\xi}) &= (1 - \xi_1)^2 F_1(\xi'_{F_1}) + (1 - \xi_2)^2 F_2(\xi') \\
&+ (1 - \xi_3)^2 F_3(\xi')(1 - \xi_4)^2 F_4(\xi') \\
&- (1 - \xi_1 - \xi_2)^2 E_1(\xi') - (1 - \xi_1 - \xi_3)^2 E_2(\xi') \\
&- (1 - \xi_1 - \xi_4)^2 E_3(\xi') - (1 - \xi_2 - \xi_3)^2 E_4(\xi') \\
&- (1 - \xi_2 - \xi_4)^2 E_5(\xi') - (1 - \xi_3 - \xi_4)^2 E_6(\xi') \\
&+ \xi_1^2 V_1 + \xi_2^2 V_2 + \xi_3^2 V_3 + \xi_4^2 V_4
\end{aligned}
$$

where $\boldsymbol{\xi} = (\xi_1, \xi_2, \xi_3, \xi_4)$ are barycentric coordinates and F_i, E_i, and V_i correspond to faces, edges, and vertices.

Results

Curved elements implemented in Nektar++, a high-order finite element code.

Meshes are identical except for boundary surfaces and tets.

Accuracy is measured in the L_2 and L_∞ norm of solution and L_2 norm of solution gradient.

$$
\begin{aligned}
L_2(u^{h,p}) &= \left(\int_{\Omega_M} (u^{h,p} - u_{exact})^2 \, \mathrm{d}\Omega_M \right)^{1/2} \\
L_\infty(u^{h,p}) &= \max_{\Omega_M} \left| u^{h,p} - u_{exact} \right| \\
L_2(\nabla u^{h,p}) &= \left(\int_{\Omega_M} \nabla(u^{h,p} - u_{exact}) \cdot \nabla(u^{h,p} - u_{exact}) \, \mathrm{d}\Omega_M \right)^{1/2}
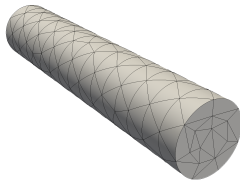\end{aligned}
$$

Hagen-Poiseuille Flow

Fully developed, laminar viscous flow through a cylindrical pipe of unit radius and length of 10 in the z- direction

$$u_z(\mathbf{x}) = -\frac{1}{4\nu}\left(\frac{\mathrm{d}p}{\mathrm{d}z}\right)(R^2 - r^2), \quad p(\mathbf{x}) = 1 - \frac{z}{10}, \quad r^2 = x^2 + y^2$$

with $u_x = u_y = 0$, $\nu = 0.025$, such that $u_z = 1 - r^2$.

Initial mesh of 941 elements.

	interp. error.
C^0	1.19×10^{-5}
G^1	6.32×10^{-3}

Hagen-Poiseulle Flow

x-velocity

	p	$L_2(u^{h,p})$	$L_\infty(u^{h,p})$	$L_2(\nabla u^{h,p})$
C^0	5	8.57×10^{-4}	6.34×10^{-3}	6.34×10^{-3}
G^1	5	1.67×10^{-3}	1.36×10^{-2}	1.36×10^{-2}
C^0	6	3.10×10^{-4}	2.43×10^{-3}	2.43×10^{-3}
G^1	6	1.65×10^{-3}	1.30×10^{-2}	1.30×10^{-2}

Accuracy of G^1 dominated by geometric error.
$y-$velocity results are similar.

Hagen-Poiseulle Flow

Pressure

	p	$L_2(p^{h,p})$	$L_\infty(p^{h,p})$	$L_2(\nabla p^{h,p})$
C^0	5	1.71×10^{-3}	2.40×10^{-2}	5.50×10^{-2}
G^1	5	4.51×10^{-3}	$\mathbf{5.25 \times 10^{-3}}$	$\mathbf{2.75 \times 10^{-2}}$
C^0	6	4.40×10^{-4}	6.85×10^{-3}	2.12×10^{-2}
G^1	6	4.47×10^{-3}	$\mathbf{4.61 \times 10^{-3}}$	$\mathbf{1.77 \times 10^{-2}}$

G^1 has lower error in several norms, but far from conclusive.

Conclusions

For a simple flow problem, G^1 continuous surface patches do not significantly improve solution accuracy compared to similar C^0 continuous patches.

The increased interpolation error of G^1 triangles appears to outweigh the potential benefits.

Other Lessons

Geometric continuity is far from the only factor; there are relevant metrics to investigate, such as the scaled Jacobian.

The effect of curvature may also play a role, to achieve G^1 continuity, the derivatives may have to change rapidly to match direction on triangle edges.

Future Work on Surface Continuity

Future work includes applying G^1 continuous boundary representations to other problems, examining its effect on forces, stresses, and other engineering quantities.

If there is shown to be a significant advantage, fifth order and higher G^1 triangles will be investigated.

Current Research

Determining curved element validity and analyzing quality using Bézier properties.

Previous work (Remacle and others) introduced an adaptive check using Bézier subdivision.

We are investigating an elevation based adaptive check, studying and comparing the two algorithms.

Current Research

With a robust and efficient validity check in place, we can move forward and extend local mesh modification operators to arbitrary order Bézier elements for mesh adaptation and quality improvement:

- Refinement (splits), with subdivision
- Coarsening (collapses), with degree reduction
- Reshaping (control point movement), with convex hull property

Investigate variable-order meshes - i.e. highest order on the boundary, lowest order on in the interior.